Earth Surface Processes and Landforms
Earth Surf. Process. Landforms **31**, 736–749 (2006)
Published online 17 November 2005 in Wiley InterScience (www.interscience.wiley.com). **DOI:** 10.1002/esp.1274

Representing the bed roughness of coarse-grained streams in computational fluid dynamics

Shaun K. Carney,[1] Brian P. Bledsoe[2]* and Daniel Gessler[3]

[1] *Riverside Technology, Inc., 2290 East Prospect Road, Suite 1, Fort Collins, CO 80525, USA (formerly at the Engineering Research Center, Department of Civil Engineering, Colorado State University, Fort Collins, CO 80523, USA)*

[2] *Department of Civil Engineering, Colorado State University, Engineering Research Center, 1320 Campus Delivery, Fort Collins, CO 80523, USA*

[3] *Alden Research Laboratory, Inc., 30 Shrewsbury Street, Holden, MA 01520-1843, USA*

**Correspondence to:*
B. P. Bledsoe, Department of Civil Engineering, Colorado State University, Engineering Research Center, 1320 Campus Delivery, Fort Collins, CO 80523. E-mail: bbledsoe@engr.colostate.edu

Received 20 October 2004;
Revised 5 May 2005;
Accepted 6 June 2005

Abstract

Computational fluid dynamics (CFD) applications are increasingly utilized for modelling complex flow patterns in natural streams and rivers. Although CFD has been successfully implemented to model many complex flow situations in natural stream settings, adequately characterizing the effects of gravel and cobble beds on flow hydraulics in CFD is a difficult challenge due to the scale of roughness lengths and the inadequacy of traditional roughness representations to characterize flow profiles in situations with large roughness elements. An alternative method of representing gravel and cobble beds is presented. Appropriate drag forces associated with different grain sizes are computed and included in the momentum equations to account for the influence of a hydraulically rough bed. Comparisons with field measurements reveal reasonable agreement between measured and modelled profiles of spatially averaged velocity and turbulent kinetic energy, and model fidelity to the non-logarithmic behaviour of the velocity profiles. The novel method of representing coarse beds expands the utility of CFD for investigating physical processes in natural channels with large bed roughness. Copyright © 2005 John Wiley & Sons, Ltd.

Keywords: CFD; river morphology; roughness; gravel; FLUENT

Introduction

Computational fluid dynamics (CFD) modelling is a powerful tool for investigating a wide variety of complex flow patterns in natural streams. Several researchers have recently demonstrated the utility of using CFD in natural stream settings (e.g. Bradbrook *et al*., 1998; Lane *et al*., 1999; Nicholas and Sambrook-Smith, 1999; Booker *et al*., 2001; Booker, 2003; Ferguson *et al*., 2003; Nicholas and McLelland, 2004). However, there are a number of difficulties associated with CFD modelling in natural settings. In particular, appropriate turbulence modelling and treatment of roughness effects near solid boundaries present challenges to the modeller (Nicholas, 2001). Directly adjacent to solid boundaries, the flow exhibits laminar characteristics that are quickly overcome by the turbulent flow characteristics away from the boundary. A zone exists outside of the laminar zone where the flow follows a semi-logarithmic relationship between velocity and distance from the wall when flow separation is weak, referred to as the 'law of the wall'. In CFD modelling, wall functions based on the law of the wall are typically utilized to transition from the no-slip conditions at the wall into the turbulent flow away from the wall rather than resolve the entire flow field adjacent to a solid boundary. The effects of wall roughness have been studied extensively for controlled, man-made systems. The typical treatment of wall roughness in CFD parameterizes the shift in the velocity profile created by wall roughness using a roughness length, k_s (e.g. Cebeci and Bradshaw, 1977).

In natural settings, boundaries are highly non-uniform, commonly composed of sediment of various sizes. It would be impractical to model the boundary following the topography of individual clasts constituting the bed of the channel under most circumstances. If boundary-fitted coordinates were defined following the complex topography created by individual clasts, the near-boundary cells would be highly distorted, causing numerical diffusion, solution stability and convergence issues (Nicholas, 2001; Lane *et al*., 2004). Alternatively, the effects of natural boundaries might be

accounted for by incorporating the influence of the non-uniform boundary into the roughness length. Many field studies have related the total roughness length k_s to a particle diameter at a certain percentile of the grain size distribution of natural streams; for instance, $k_s \approx 3{\cdot}5D_{84}$ or $k_s \approx 6{\cdot}8D_{50}$ (Hey, 1979; Bray, 1982). However, there are substantial limitations of utilizing large roughness lengths that affect the accuracy and stability of solutions. Utilizing a roughness length in situations with larger roughness elements presents challenges for CFD modelling (Nicholas and Sambrook-Smith, 1999; Lane *et al*., 2004) as the roughness length is constrained to half the near-bed cell thickness (Fluent Inc., 2003). If the relationship $k_s = 3{\cdot}5D_{84}$ is used to set the roughness length, then the thickness of the first cell above the bed would have to be at least seven times the D_{84} grain size. This is impractical for beds composed of cobbles or even gravels because of the constraints on the amount of flow detail that could be resolved in streams with larger grain sizes. Solution stability and solution accuracy become problematic (Nicholas and Sambrook-Smith, 1999). If large near-bed cells were used, the cell centroid may no longer fall within the law of the wall region (in the lower 20 per cent of the flow; Wilcock, 1996). Thus, it is not possible to model the roughness associated with larger grain sizes utilizing standard roughness length representations.

Nicholas (2001) attempted to overcome these obstacles using a combination of boundary-fitted coordinates and appropriate roughness lengths to capture the effects of natural roughness on flows. Nicholas (2001) distinguished between different components of roughness in a channel. The first encompassed sub-grid-scale roughness that could be represented with a smaller roughness length, as suggested by Clifford *et al*. (1992). The second included supra-grid-scale roughness. The supra-grid-scale roughness is subdivided between large-scale roughness elements such as pool–riffle sequences and changes in planform geometry that can be resolved with a conventional field survey, and intermediate-scale roughness elements such as particle clusters and small-scale bedforms. Nicholas (2001) attempted to model the intermediate-scale roughness using a randomly varying component of the bed elevation superimposed on the large-scale channel geometry, yet found the roughness lengths required and the resulting flow solution to be highly grid dependent. He concluded that, particularly in situations with large grain sizes, this modelling strategy may be inappropriate for CFD applications to natural streams.

Lane *et al*. (2004) presented a method that is clearly superior to both boundary-fitted coordinates and a roughness length treatment of boundary roughness. High-resolution digital elevation data collected using close-range digital photogrammetry were combined with a numerical porosity treatment of the bed to model highly detailed flows that reflect the influence of individual grains on the flow field. By treating the flow field immediately above the bed as flow through porous media, orthogonal grid cells could be utilized, removing the need to use boundary-fitted coordinates, an important source of solution instability, numerical diffusion and grid-dependent solutions. The methodology is also highly conducive to modelling erosion and deposition. Although Lane *et al*. (2004) suggest that the statistical characteristics of a gravel bed could be utilized to extend this work to larger scales (e.g. Butler *et al*., 2001), they also acknowledge the computational limitations of modelling at such a high resolution. In its current form, implementing the Lane *et al*. (2004) method would require modifications to existing CFD software packages to iteratively compute wall roughness heights in individual cells based on the porosity of the cell, as well as the technological capabilities to implement close-range digital photogrammetry to produce the digital elevation model (DEM) input data. The method has recently been modified for application at larger spatial scales (S. N. Lane, personal communication, 2005). Although the techniques employed by Lane *et al*. (2004) offer the potential of resolving highly detailed flow fields over gravel beds, this level of detail typically is not required.

The effects of natural boundary roughness can also be incorporated into CFD modelling utilizing drag force concepts. This approach has been widely developed in atmospheric sciences (Raupach and Shaw, 1982) and applied to simulate flows through synthetic and natural vegetation in open channel flow scenarios (Shimizu and Tsujimoto, 1994; Lopez and Garcia, 1997; Fischer-Antze *et al*., 2001; Nicholas and McLelland, 2004). Olsen and Stokseth (1995) developed a method for accounting for large-scale roughness elements using drag force concepts, although the method is based on porous groundwater flow equations (Engelund, 1953). Recently, Nicholas (2005) developed a drag force representation of bed roughness where the drag coefficients are based on bed topography profiles. The Nicholas (2005) methodology appears to effectively represent bed roughness, although bed topography profiles are not easily collected.

In this paper, a method for representing natural, hydraulically rough beds containing mixtures of gravels and cobbles is presented. The method draws on the theoretical work of Wiberg and Smith (1991) and treats the bed as a porous medium. The drag coefficients associated with the porous medium are computed based on observed grain size distributions. The method provides a straightforward, yet physically based treatment of bed roughness in natural streams. In addition, the FLUENT 6.1 CFD package used in this study contains models that may be readily adapted to apply this method, avoiding the introduction of code modifications through user-defined functions (Fluent Inc., 2003). The proposed method is applied to compute spatially averaged flow profiles, and the resulting simulations are compared with flow profiles and the observations of previous researchers. Finally, some of the potential applications of the method are discussed.

Methods

The approach proposed by Wiberg and Smith (1991) for representing spatially averaged velocity profiles over streambeds composed of gravels and cobbles is modified for use in finite-volume CFD. In this method, drag forces associated with different grain sizes are computed and aggregated as a sink in the momentum equations. The treatment of the bed is analogous to modelling a porous zone on the bed.

Wiberg and Smith (1991) computed spatially averaged velocity profiles over rough beds of well-sorted sediment by breaking the total shear stress into turbulent shear stress and shear stress arising from the form drag associated with grains constituting the bed of the channel. The turbulent shear stress is computed using a modified form of a mixing length turbulence model. Form drag values corresponding to grain classes are computed and summed at different levels above the bed and are used to compute drag-related shear stresses. In this paper, a similar treatment of the bed is developed to include the form drag of the bed in the momentum equations for use in a finite-volume setting. The mixing length turbulence model is replaced with the renormalization group theory (RNG) k–ε turbulence model (Yakhot and Orszag, 1986).

Wiberg and Smith (1991) begin with a number of assumptions. (1) The bed is assumed to be composed of well-sorted, randomly distributed grains whose concentration in the bed is proportional to their frequency in the grain size distribution. (2) All the grains in the active layer of the bed affecting the flow are positioned within the layer with the bottom of each grain resting on a single plane, i.e. all grains have a common zero elevation. Although this assumption is not necessary for the drag computations, it is supported by field observations (Wiberg and Smith, 1991) and simplifies the computations. (3) The grains constituting the bed are assumed to have their short axes vertically aligned, as is typical in natural streams (Limerinos, 1970; Marchand *et al.*, 1984). (4) Particles are treated independently of each other, and therefore shadowing effects are neglected. (5) The role of roughness element spacing is neglected. (6) The effects of flow blockage are assumed to be adequately captured in the drag forces. Although each of the last three assumptions plays an important role in sediment transport and roughness computations, the relative importance of these factors is assumed to be dominated by the computed drag forces. In addition, the assumptions may have offsetting effects. The impact of these assumptions is considered in the discussion.

Because the Wiberg and Smith (1991) drag model is modified for use in a finite-volume CFD code, it is necessary to compute drag forces per unit volume associated with the different grains of the bed. The drag force averaged over the height of a single grain of size fraction (D_m) is computed as:

$$(F_D)_m = \frac{\rho}{2}(C_D)_m(A_D)_m\langle u^2\rangle \tag{1}$$

where $(C_D)_m$ is a drag coefficient, $(A_D)_m$ is a grain's cross-sectional area perpendicular to the flow direction, and $\langle u^2\rangle$ is the average of the squared velocity. Alternatively, the drag force at a level z between the top and bottom of a grain, $(F_D(z))_m$, could be computed by replacing the average velocity with the velocity at the height z, $u(z)$, in Equation 1. The grain's cross-sectional area perpendicular to the flow is assumed to be:

$$(A_D)_m = \frac{\pi}{4}D_{my}D_{mz} \tag{2}$$

and the volume over which this force acts is equal to the volume of the grain, or:

$$(V_D)_m = \frac{\pi}{6}D_{mx}D_{my}D_{mz} \tag{3}$$

when the grain shape is assumed to be elliptical. The subscripts x, y, and z in Equations 2 and 3 refer to the downstream, cross-stream, and vertical grain dimensions, respectively. The concentration of grains of a specific grain size fraction, c_m, is used to compute the average drag force of that grain acting over the entire bed. Because the bed is composed of a range of grain sizes, the total drag force at a given level above the bed is summed over the grain sizes affecting the flow at that level:

$$\frac{F_{D,total}(z)}{V_{total}} = \sum_{m=l}^{M} c_m\left(\frac{F_D(z)}{V_D}\right)_m \tag{4}$$

where $F_{D,total}(z)$ is the total drag force at height z and V_{total} is the volume of fluid over which this drag force acts. The grain size (D_l) refers to the smallest grain size at level z, whereas D_M refers to the largest grain in the grain size distribution. Substituting Equations 1, 2 and 3 into 4 yields:

$$\frac{F_{D,total}(z)}{V_{total}} = \sum_{m=l}^{M} c_m \frac{\frac{\rho}{2}(C_D)_m\left(\frac{\pi}{4}D_{my}D_{mz}\right)}{\frac{\pi}{6}D_{mx}D_{my}D_{mz}}u(z)^2 = \frac{3}{4}\rho\sum_{m=l}^{M} c_m \frac{(C_D)_m}{D_{mx}}u(z)^2 \tag{5}$$

In FLUENT, it is possible to include a momentum sink term with a similar form to Equation 5 through the use of a porous-medium zone. The momentum sink associated with inertial resistance for a homogeneous porous medium is modelled in FLUENT (Fluent Inc., 2003) as:

$$S_i = C_2\frac{1}{2}\rho u_{mag}u_i \tag{6}$$

where S_i is the ith (x, y or z) momentum equation sink term, C_2 is the inertial loss coefficient (L^{-1}), u_{mag} is the velocity magnitude, and u_i is the velocity in the x, y or z direction. For flow limited to the downstream direction, Equations 5 and 6 can be equated and simplified to relate the inertial loss coefficient (C_2) to the grain drag:

$$C_2(z)\frac{1}{2}\rho[u(z)]^2 = \frac{3}{4}\rho\sum_{m=l}^{M} c_m \frac{(C_D)_m}{D_{mx}}[u(z)^2] \tag{7}$$

which reduces to:

$$C_2(z) = \frac{3}{2}\sum_{m=l}^{M} c_m \frac{(C_D)_m}{D_{mx}} \tag{8}$$

Thus, the inertial loss coefficient (C_2) at a given elevation z above the bed may be computed based on the drag coefficient, concentration and grain diameter in the downstream direction of grains above the elevation z.

The concentration of the grains may be computed by assuming a log-normal distribution for the grain sizes:

$$c_m = \frac{c_b}{\sigma(2\pi)^{1/2}}\exp\left[-\frac{1}{2}\left(\frac{\phi_m - \phi_{50}}{\sigma}\right)^2\right] \tag{9}$$

where $\phi = -\log_2(D)$ for D (in mm), ϕ_{50} is the median grain size (in ϕ units), σ is the standard distribution of the grain sizes (in ϕ units), and c_b represents the maximum concentration of particles in the bed, or the inverse of the average porosity of the bed. Observations indicate that c_b typically takes a value of about 0·6, which is used in this model (Wiberg and Smith, 1991).

In the original Wiberg and Smith (1991) model, the drag coefficient (C_D) is computed based on relationships between the Reynolds number and C_D for spheres (Coleman, 1967). For the range of Reynolds numbers between about 10^3 to 10^5, however, the drag coefficient for spheres is relatively constant and equal to about 0·45. If the drag coefficient may be assumed constant rather than a function of the velocity for the range of flows of interest, then the computed value of the inertial loss coefficient would be a constant at a given elevation z, which greatly simplifies its application. Wiberg and Smith (1991) computed velocity profiles with their model using the average drag coefficient, $C_D = 0{\cdot}45$. The results were very similar to the profile using a variable value of C_D in both shape and magnitude. Thus for implementation in FLUENT, the drag coefficient was assumed constant and equal to 0·45.

In order to compute the summation in Equation 8, the grain size distribution is broken into a discrete series of grain sizes. In FLUENT, porous zones are created that correspond to the difference in the discrete grain heights, assuming all grains have a common zero level (see Figure 1). Thus a single value of C_2 may be computed for each zone. Beginning with the highest zone, the summation reduces to the influence of a single grain. Working down from the highest zone, at each level the influence of one additional grain size is added to the previous inertial loss coefficient until the bottom level is reached, at which point the summation includes the influence of all grain sizes in the distribution. The computed C_2 values can then be applied to each porous-medium zone in FLUENT.

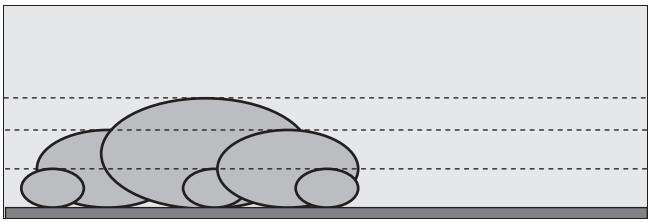

Figure 1. Drawing of the theoretical arrangement of bed particles assuming a common zero plane for all grain sizes.

Alternatively, a single grain size in the distribution may be used to represent the bed rather than the full distribution. Using a single grain size may not capture differences in sediment sorting on the velocity profile, as was demonstrated by Wiberg and Smith (1991). However, if a representative grain size could be used to compute a single inertial loss coefficient that reproduces the average effects of the bed on the velocity profile without losing appreciable accuracy in the profiles, this would be a valuable simplification. Whiting and Dietrich (1990) and Wiberg and Smith (1991) identified the D_{84} particle size as the dominant grain length scale influencing flow profiles. Therefore, for the presented results, the D_{84} grain size is used. If only the D_{84} grain size is used, the summation in Equation 8 reduces to:

$$C_2 = \frac{3c_b C_D}{2D_{84x}} \tag{10}$$

A roughness height of 0·5 mm, corresponding to medium sand, is defined to account for smaller grain roughness at the wall beneath the porous zones, consistent with Wiberg and Smith (1991). Wiberg and Smith (1991) found that this roughness length could be increased up to the D_{50} particle diameter and still have little effect on the resulting velocity profiles.

The velocity profiles computed using the above method are spatially averaged velocity profiles and, therefore, do not capture variation in flow characteristics in the bed region. In formal spatial averaging, form-induced, or dispersive, stresses arise in much the same way that Reynolds stresses arise due to temporal averaging of the Navier–Stokes equations, which, if accounted for, prevent the arbitrary addition of drag forces to the momentum equations (Nikora *et al*., 2001). In the model presented here, it is assumed that the drag created by the grains dominates the dispersive shear stresses to the extent that these shear stresses can be neglected. Therefore, the standard RNG k–ε turbulence model with standard equilibrium wall functions is utilized. Although the model runs here involve relatively simple geometry, the RNG k–ε turbulence model has been shown to perform better than the standard k–ε model in natural streams involving complex flow geometry (e.g. Bradbrook *et al*., 1998). If the approach presented here were extended to model more complex geometries, the RNG k–ε turbulence model would likely yield more accurate results.

FLUENT discretizes the governing equations using a finite-volume approach. The momentum equations and turbulence equations were discretized using second-order upwind differencing. The PRESTO (PREssure STaggering Option) pressure interpolation scheme was used, as recommended for simulations involving porous media (Fluent Inc., 2003). SIMPLEC (SIMPLE-Consistent) pressure–velocity coupling was utilized, which allowed higher under-relaxation factors (0·8 to 1·0) to be used.

The water surface was modelled using a fixed-lid approach where the free surface was simulated as a symmetry plane with normal velocity components and normal gradients of all variables equal to zero. A periodic inlet/outlet boundary condition was used to achieve a fully developed flow profile. With the periodic boundary condition, the discharge through the domain is adjusted until the slope computed, based on the downstream pressure gradient, matches the desired slope $(dP/dx)/\rho g = S_f$ (Nicholas, 2001).

Comparison with Field Measurements

Marchand *et al*. (1984) collected velocity profiles from nine streams in Colorado with relative roughness ranging from $D_{84}/h = 0{\cdot}07$ to 0·43, where h is the flow depth. Velocity profiles were collected at three or four locations along the centreline of the stream at eight to ten points in the vertical. Velocities were collected at three different stages for each site. Measurements of grain size distributions, including each of the three major axes of the grains, water surface slope, and stream depth were also made.

Wiberg and Smith (1991) used their model to simulate velocity profiles and compute average velocities for each of the nine streams at each measured stage of the Marchand *et al*. (1984) data set. To demonstrate the consistency of the authors' CFD simulations with the Wiberg and Smith (1991) model, CFD simulations were conducted for three streams representing the range of the Marchand *et al*. (1984) data set at the median of the measured stages. Before presenting the modelling results and comparisons, additional details regarding the bed representation, bed discretization, and grid independence tests are presented.

Two different CFD simulations were completed for each of the three streams. In the first, a full grain size distribution discretized into distinct bins was assumed in describing the bed. In the second, the D_{84} grain size was used to represent the entire bed. In the first simulation, zones corresponding to the difference in discretized grain heights in the vertical direction were created and defined as porous media in FLUENT. Inertial loss coefficients corresponding to each level were computed and assigned to each zone according to Equation 8. In the second simulation, the D_{84} grain size was used to compute a single inertial loss coefficient according to Equation 10, and this coefficient was assigned to a single zone the thickness of the $D_{84,z}$ axis. Consistent with Marchand *et al*. (1984) field observations and the Wiberg and Smith (1991) modelling application, the vertical grain axis (D_z) was assumed to correspond to the short grain axis and the downstream grain axis (D_x) was related to D_z according to $D_x = 2D_z$. The streams were assumed wide enough such that the influence of the banks on the velocity profiles was negligible and the streams could be modelled as infinitely wide (two-dimensional).

In the first simulation method, the grain size distribution could be discretized in different manners. Two different discretization methods were utilized and compared in preliminary tests. In the first, equal phi bins were created corresponding to different grain sizes, consistent with the Wiberg and Smith (1991) approach. In this method, the bins were concentrated near the bed, but there was less resolution higher in the flow. The determination of the bins was made independent of the grain size distribution characteristics. In the second method, ten bins of equal concentrations were created based on the grain size distribution characteristics. The bins on each tail of the grain size distribution were further subdivided to provide finer discretization at the ends of the distribution, yielding a total of 16 bins. The second discretization yielded finer divisions in the larger grain sizes than did the first discretization method.

Preliminary tests of the two discretization methods revealed minor (0 to 4 per cent) differences in velocity profiles, yet larger (0 to 15 per cent) differences in turbulent kinetic energy profiles, a measure of turbulent velocity fluctuations. Thus, the grain size discretization scheme becomes important when looking at turbulence quantities and shear stresses computed using the turbulence models, yet is relatively insignificant when looking at velocity profiles. Because of the direct connection to grain size distribution characteristics and the finer discretization of larger grain sizes for a given scenario, the second discretization method is utilized in all of the subsequent runs involving the full grain size distribution.

One common difficulty in CFD modelling involves the determination of grid independence. The uncertainty in the simulated results due to the grid resolution was quantified through a series of grid refinement tests following Hardy *et al*. (2003). Because the flow solutions utilize the periodic boundary condition and are fully developed, the grid resolution in the downstream direction does not impact the flow profiles. Grid resolution dependency was tested for one scenario representing the bed using the grain size distribution and another representing the bed with the single D_{84} grain size. The stream with the highest velocities and relative roughness modelled in this study was used for the tests. Model runs were made with three different grids with the vertical resolution approximately doubled in each subsequent run. The coarse, medium and fine resolution grids contained 17, 29 and 56 cells in the vertical direction, respectively, for the runs with the grain size distribution, and 15, 26 and 48 cells, respectively, for the runs representing the bed using the single D_{84} grain size. Downstream velocity and turbulent kinetic energy were compared at common points for the three grids, and the mean absolute percentage differences between the variables were computed, assuming the finer resolution grid yielded the more accurate solution (Table I). The differences between model

Table I. Mean absolute percentage differences between simulated flow variables for grids of different resolution at common grid points

Bed representation	Grids	u_x	*tke*
Full distribution	Coarse and medium	0·2	2·4
Full distribution	Medium and fine	0·2	0·6
Only D_{84}	Coarse and medium	0·7	4·4
Only D_{84}	Medium and fine	0·2	1·3

u_x is the velocity in the downstream direction and *tke* is the turbulent kinetic energy.

Table II. Stream characteristics and average velocities for three river simulations

Data set	Clear Creek at Golden	Blue River near Dillon	Lake Creek
Bed slope	0·006	0·013	0·029
$D_{84,c}$ (mm)	111	105	255
Standard deviation of the grain size distribution (ϕ units)	1·3	1·1	1·1
$D_{84,c}/h$	0·09	0·17	0·27
Range of $\bar{u}$ measured by Marchand *et al.* (1984) (cm s^{-1})	193–250	161–213	140–285
$\bar{u}$ for Wiberg and Smith (1991) model (cm s^{-1})	200	195	287
$\bar{u}$ for FLUENT simulation with grain size distribution (cm s^{-1})	200	191	285
$\bar{u}$ for FLUENT simulation with single D_{84} grain size (cm s^{-1})	187	177	264

$D_{84,c}$ is the 84th percentile short (vertical) axis grain diameter.

results from the different grids are minor. The subsequent model runs were completed with a resolution similar to the medium resolution meshes used in the grid refinement tests (between 25 and 30 cells vertically).

As stated, CFD simulations were conducted for three streams representing the range of the Marchand *et al*. (1984) data set at the median of the measured stages using the two different bed configurations. Average velocities were then computed consistent with Marchand *et al*. (1984). Simulated mean velocities were virtually identical to those computed by Wiberg and Smith (1991) using the grain size distribution. Mean velocities computed using the single D_{84} grain size were approximately 92 per cent of the Wiberg and Smith (1991) average velocities. Stream characteristics and average velocities are shown in Table II.

Modelled velocity profiles from the same three streams were presented in Wiberg and Smith (1991). For each stream, the three to four velocity profiles measured along the centreline at each stage were averaged for comparison with the spatially averaged profiles computed using their model. CFD simulations of each of these streams were performed at the mean of the stages measured by Marchand *et al*. (1984), as done by Wiberg and Smith (1991). For consistency with Wiberg and Smith (1991), the stages were adjusted to account for the differences between the measured bed at the top of grains and the zero-velocity plane assumed to be located within the bed by adding $0{\cdot}5D_{50}$ to the mean stage. This adjustment had minor effects on the resulting profiles. As described above, separate CFD simulations were made using the grain size distribution and using a single D_{84} grain size to represent the bed.

Figure 2 shows the resulting profiles, the range of averaged data collected by Marchand *et al*. (1984), Wiberg and Smith (1991) model results, CFD simulation results using the grain size distribution, and CFD simulation results using D_{84} to represent the bed. A logarithmic velocity profile is also plotted for comparison. The logarithmic velocity profile is computed external to CFD using the equation (Hey, 1979):

$$\frac{u}{u_*} = \frac{1}{\kappa} \ln\left(\frac{z}{z_0}\right) \tag{11}$$

where κ is the von Karman constant, u is the velocity at height z above the bed, z_o is the height corresponding to $u = 0$, $z_o = k_s/30$ (Nikuradse, 1933) and $k_s = 3{\cdot}5D_{84}$ (Hey, 1979), u_* is the shear velocity, defined as $u_* = (\tau_o/\rho)^{1/2} = \sqrt{(gRS_f)}$, wherein a consistent set of units τ_o is the cross-section-averaged shear stress, ρ is the fluid density, g is the acceleration due to gravity, R is the hydraulic radius, and S_f is the friction slope, commonly approximated as the bed slope (S_o). It should be emphasized that a logarithmic velocity profile could not be computed in CFD based on the roughness length due to the computational limitations discussed in the introduction.

The root mean squared error (RMSE) is computed for each of the simulated velocity profiles relative to the average of the Marchand *et al*. (1984) velocity profiles. These results are presented in Table III. The results indicate that in the first and third cases, the CFD simulations better capture the average velocity characteristics compared with the logarithmic velocity profile. In the second case the CFD models perform equally well and provide a better fit below $0{\cdot}6\ h$ (Figure 2).

The characteristic S-shape of the profile for the streams with relative roughness up to 0·30 has been captured in the CFD simulations. In the lower 10 to 40 per cent of the flow profile, the simulated velocities are up to 25 per cent higher than those reported using the original Wiberg and Smith (1991) model, with the greatest differences in the near-bed region for the streams with higher relative roughness. In the upper half of the flow profiles, velocities using the modified Wiberg and Smith models are 5 to 10 per cent lower than those using the original Wiberg and Smith (1991)

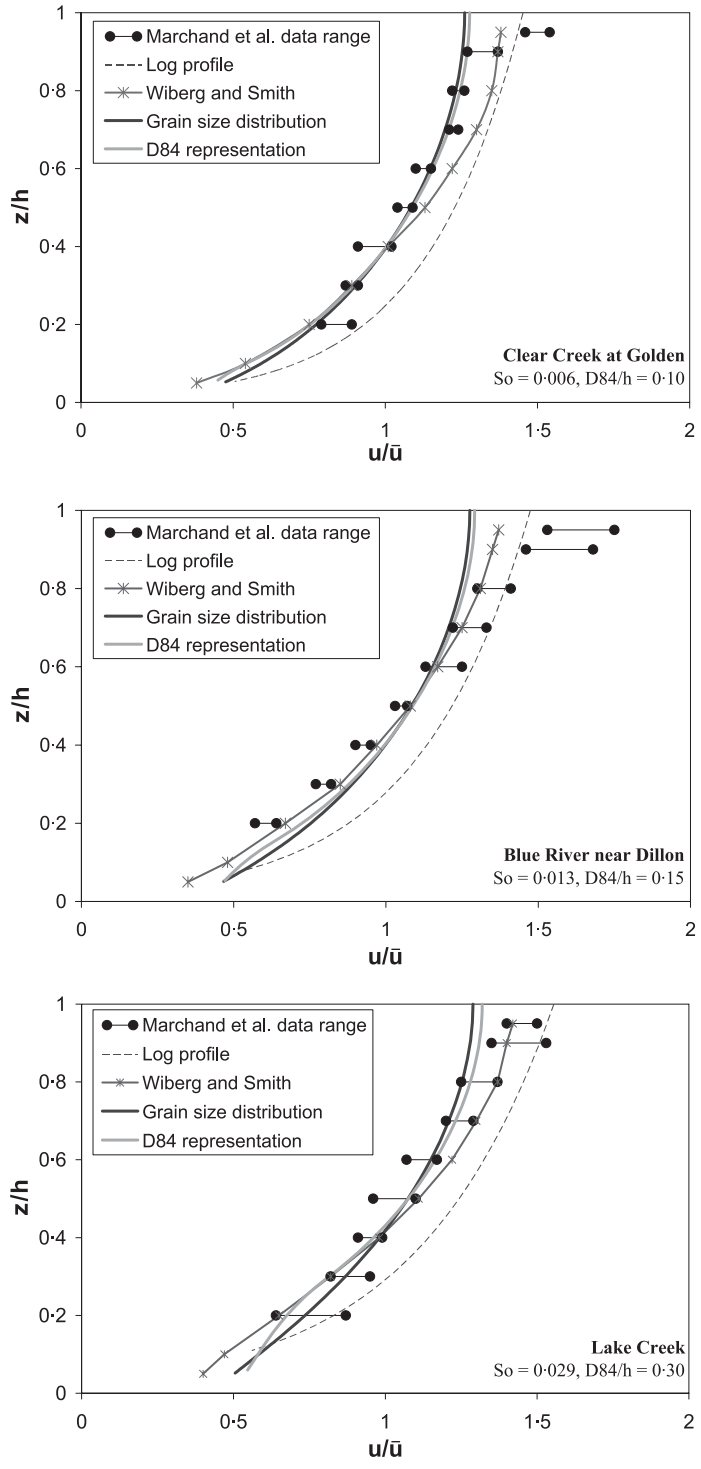

Figure 2. Velocity profiles for three streams comparing model results and field data from Marchand *et al.* (1984).

Table III. Root mean squared error (RMSE) between simulated velocity profiles and the mean of the three spatially averaged velocity profiles measured by Marchand *et al.* (1984). Data were compared between points at the same relative depth of flow for each profile

		CFD (this study)		
Data set	Wiberg and Smith	Full distribution	Only D_{84}	Log profile
Clear Creek at Golden	0·08	0·09	0·08	0·14
Blue River near Dillon	0·13	0·19	0·17	0·18
Lake Creek	0·07	0·08	0·08	0·15

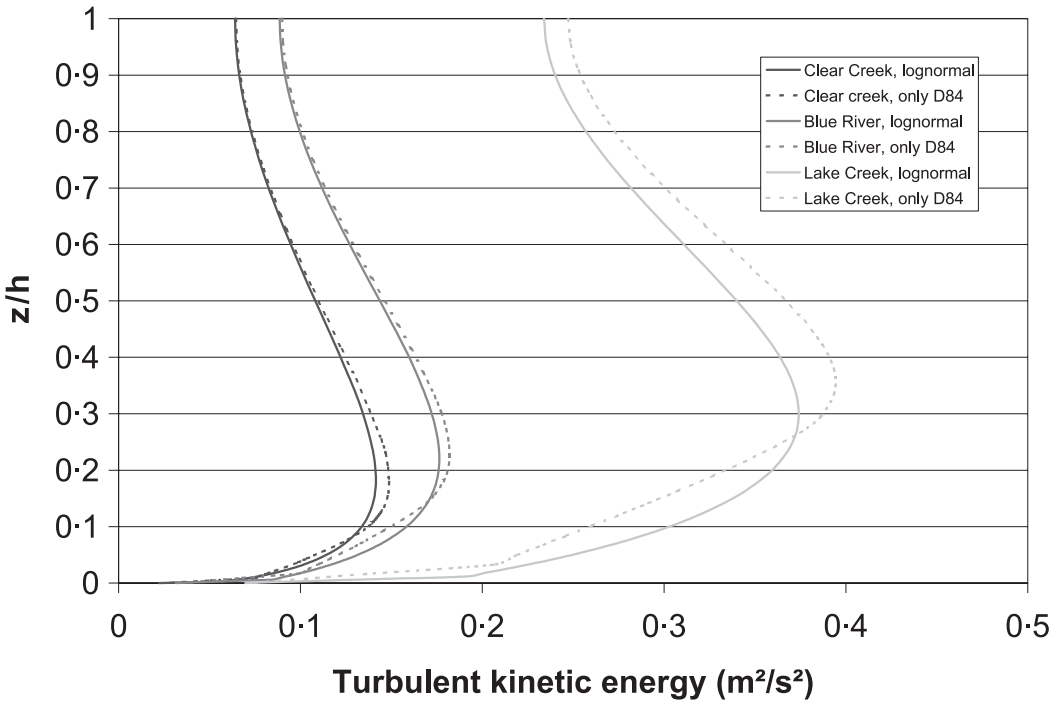

Figure 3. Comparison of turbulent kinetic energy profiles for the modelled streams shown in Figure 2. Solid lines indicate simulations using the grain size distribution and dashed lines indicate simulations using the D_{84} grain size to represent the bed.

model. The modified Wiberg and Smith approach and the original Wiberg and Smith (1991) model give similar results relative to the field data, as evidenced by similar RMSE statistics.

Comparing flow profiles simulated using the grain size distribution and the D_{84} grain size, the differences in the profiles are minor relative to differences with the other profiles. The largest differences are in the vicinity of the bed, where the flows of the simulation using the D_{84} grain size are retarded 6 to 9 per cent from those of the simulation using the grain size distribution. At approximately $z/h = 0{\cdot}5$, the two profiles cross and the simulations using the D_{84} grain size predict higher velocities, as expected given the lower velocities near the bed.

Turbulent kinetic energy, a measure of the magnitude of velocity fluctuations in the flow, is modelled in this study with the RNG k–ε turbulence model. Turbulent kinetic energy profiles using the grain size distribution and the D_{84} grain size representation of the bed are plotted for each modelled stream in Figure 3. No measures of velocity fluctuations were reported in the Marchand *et al.* (1984) study for comparison. The steeper streams have higher turbulent kinetic energy. The turbulent kinetic energy has a peak between 0·14 and 0·34 h, depending on the stream and the bed representation. In the streams with higher relative roughness, the peak of the turbulent kinetic energy is higher in the flow. The simulations using a single grain size to represent the bed also result in a turbulent kinetic energy peak 3 to 5 per cent higher than the simulations using the grain size distribution.

Discussion

The method of representing hydraulically rough gravel and cobble beds presented in this paper appears to reasonably represent spatially averaged flow characteristics in streams with relative roughness up to $D_{84}/h = 0{\cdot}30$. CFD wall functions that rely on a roughness length to represent bed resistance have limited applicability due to modelling inaccuracies in situations with large relative roughness and associated grid resolution limitations. This relatively simple treatment of the bed removes the constraints imposed by relying on a roughness length and opens the potential to implement commercial CFD modelling in gravel- and cobble-bed streams.

The resulting velocity profiles show the same basic characteristics as those computed by Wiberg and Smith (1991), but differ slightly high in the flow and in the bed region due to three modifications of the Wiberg and Smith (1991) method. First, in the original method, the drag coefficient (C_D) was computed for a sphere as a function of the grain size Reynolds number. In the CFD implementation, however, a constant value of C_D is assumed regardless of the Reynolds number. Second, the drag force for each grain size was computed in the original method using the average velocity over the grain, whereas local velocities were used in the CFD implementation. Finally, a zero-equation mixing length turbulence model was used by Wiberg and Smith (1991), whereas the two-equation RNG k–ε turbulence model was used in the CFD implementation. Differences in flow profiles between the original and modified approaches are most likely primarily due to differences in turbulence closure. In the bed region, however, where the Wiberg and Smith (1991) model yields lower velocities than the CFD implementation, differences may be due in part to treatment of the drag coefficient. In the near-bed region, the Reynolds number is lower, and if less than about 10^3, the drag coefficient would be higher than the average value of 0·45 assumed in the modified profile. If a higher drag coefficient were applied close to the bed, velocities would be reduced and the profile would more closely match those computed by Wiberg and Smith (1991). The scatter of data in the near-bed region and lack of measurements closer to the bed prevent a clear determination of whether one method more accurately portrays the velocity characteristics near the bed.

Comparing the velocity profiles to the field data, the largest consistent differences occur near the water surface, as was the case with the original Wiberg and Smith (1991) model. The differences may be attributed to some extent to a lack of detailed information concerning the field sites, but more likely may be attributed to some of the assumptions made during model development. Potentially the most important effect that is neglected by the current model is the impact of flow blockage by grain particles. The model incorporates a sink term in the momentum equations to represent the drag force, but does not include a corresponding term in the continuity equation to account for the portion of a cell containing bed material. The impact of flow blockage would be to reduce the amount of flow volume passing through the zones containing bed material. If the depth of flow were kept constant in the modelled velocity profiles, accounting for this effect would likely yield an increase in flow velocity higher in the flow profile, which could subsequently improve the fit of the simulated velocity profiles. It is difficult to determine if the shape of the near-bed velocity profiles is good, given the lack of near-bed velocity measurements.

Two other assumptions could significantly impact the flow profiles in different situations. First, particle shadowing effects were neglected and particles were modelled assuming the entire frontal area was exposed to the flow. The extent that a given clast is protected by another is a function of its relative size and arrangement in the bed. This assumption therefore overestimates the area over which the drag forces are applied. These effects would be difficult to explicitly account for, although they may be important depending on the question being investigated. For instance, shadowing effects would play an important role in an investigation of flow–sediment interactions related to sediment sorting.

The current model implicitly assumes that as roughness element spacing increases, the associated drag also increases. However, Nowell and Church (1979) demonstrated that maximum roughness occurs at intermediate roughness concentrations and that as the ratio of roughness height to element spacing gets very large, the effective roughness declines. The impact of these effects is not apparent in the data sets used in this investigation, but may be identified as an important factor if additional data sets are investigated.

Although each of the above indicates potential limitations of the modelling technique, it appears that the different assumptions offset each other to some degree and are relatively minor compared to the overriding influence of the drag associated with the bed particles. One of the primary goals of this research was to develop a relatively straightforward method that could be readily applied in CFD applications (specifically FLUENT) without code modifications. The above effects would require the use of user-defined functions for application in FLUENT and would be relatively difficult to parameterize, and were therefore neglected. These potentially could be incorporated into future refinements of the present model.

The comparable accuracy of the original Wiberg and Smith (1991) model and the modified CFD implementation demonstrates that the simplified turbulence model used by Wiberg and Smith (1991) provides a good closure for less complex geometries such as those modelled here. There is no clear benefit to using a more complex turbulence closure

for these cases. However, the RNG k–ε turbulence model would likely perform better in simulating flows involving more complex geometries than the mixing length eddy viscosity model used by Wiberg and Smith (1991), although with increasingly complex channel geometries, the spatially averaged velocity profiles produced by the CFD drag force implementation could limit its applicability for modelling.

Comparing the flow profiles from simulations using the grain size distribution to those based on the D_{84} grain size, the differences in velocity profiles are minor. The overall drag exhibited by representing the bed using only the D_{84} grain size is slightly higher than the drag of the bed using the grain size distribution, as demonstrated by the slightly lower average velocities. The effects of the higher drag can be seen in the vicinity of the bed, where the flows are retarded slightly more with the simulation using a single D_{84} grain size than with the simulation using the grain size distribution. Again, for the three streams that were modelled, it was not clear that one method yields better results than the other, except possibly for the situation with the largest relative roughness (Lake Creek, $D_{84}/h = 0{\cdot}3$). In the Lake Creek simulations, it appears the grain size distribution bed representation better simulates the flow profile. This suggests that for larger relative roughness, the effects of sediment sorting and the other grain sizes become important, which are more clearly represented in the model using the grain size distribution. Bathurst *et al*. (1981) specified three ranges of relative roughness corresponding to different flow characteristics, with divisions at approximately $D_{84}/h = 0{\cdot}25$ and 0·83. The lower division ($D_{84}/h = 0{\cdot}25$) corresponds roughly to the point where the simulations involving the grain size distribution may yield better resulting flow profiles. Additional data and research could clarify at what point sediment sorting becomes critical and a single grain size would no longer adequately characterize the flow profiles. The above results also indicate, however, that utilizing the model with only the D_{84} grain size rather than the entire grain size distribution can yield very similar results and provide an attractive simplification for application in modelling.

Wiberg and Smith (1991) demonstrated that as the relative roughness decreases, the velocity profiles utilizing their methodology approach the logarithmic velocity profile. At some small relative roughness, the standard wall function approach utilizing a roughness length would yield results with a similar level of accuracy as the porosity treatment of the bed in CFD, and grid resolution limitations would not create a prohibitive constraint. The precise level at which the porous bed treatment should be utilized is unclear and is partially dependent upon the level of flow detail desired in the near-bed region. In addition, in situations with relative roughness greater than those in this study, the porous bed treatment of boundary roughness may no longer yield accurate or meaningful results as the clasts composing the channel affect the flow to a greater extent and cause more complex flow interactions. For the streams modelled in this study ($0{\cdot}10 < D_{84}/h < 0{\cdot}30$), the computed flow profiles were all clearly superior to the standard log law velocity profile, yet no streams outside of this range were studied. Further research could clarify the lower relative roughness limit of applicability of the porous bed treatment of roughness (or the upper limit of the usefulness of standard wall function approaches), as well as the upper limit of the porous bed treatment.

In the Lane *et al*. (2004) model, where a porosity treatment of the bed is combined with high-resolution DEM data, an important advance was made with respect to the simulation of turbulence and shear stress in the vicinity of the bed. Lane *et al*. (2004) noted a zone of high turbulent kinetic energy at approximately 0·2 h, consistent with flume and field observations that peak turbulent kinetic energy occurs above the bed at an elevation controlled by the height of the particles that protrude farthest into the flow. The porosity treatment of bed roughness employed in the present study yields an upward displacement of peak turbulent kinetic energy values to elevations between 0·14 h and 0·34 h that vary systematically with relative roughness among the three streams. The forms of the turbulent kinetic energy profiles in Figure 3 are consistent with flume and field data which demonstrate that peak turbulence intensities typically occur above the bed near the top of roughness elements in the range 0·1 h–0·5 h (Wang *et al*., 1993; Buffin-Belanger and Roy, 1998; Lawless and Robert, 2001; Nicholas, 2001). In contrast, CFD models based on the wall function approach do not reproduce this behaviour and instead predict turbulence intensities to peak at the bed and decline monotonically towards the water surface (Nicholas, 2001, 2005).

Although accurate representation of velocity profiles is a worthwhile goal of CFD modelling, the key goal related to sediment transport is the accurate representation of the shear stresses on the bed of the channel. The data sets investigated do not provide the information needed to quantify the rate of change of near-bed velocities or turbulent quantities. However, the general shape of the turbulent kinetic energy profiles does better match field observations, so one would subsequently expect improved estimation of shear stresses. The shear stress in the fluid at any point may be estimated from turbulence quantities computed in CFD (Lane *et al*., 1999). This could potentially be done at a certain level above the bed, such as at a level corresponding to the top of the D_{84} grain size, to quantify average shear stresses on the bed of a stream.

In addition to identifying a peak in turbulent kinetic energy near 0·2 h that is controlled by the height of the most protruding bed particles, Lane *et al*. (2004) found that their models reproduced relatively high turbulent kinetic energy values in the vicinity of the bed due to the flow around individual grains. High values of turbulent kinetic energy near

the bed are not produced by the modified Wiberg and Smith model. These high values are the result of the complex flow patterns and high-velocity gradients as the flow moves over and around individual grains near the bed, resulting in shear stresses in the fluid. Nikora *et al*. (2001) found these form-induced shear stresses were largest in the region below the crests of the largest grains. The proposed model assumes that the effect of these shear stresses is negligible relative to the effect of the drag created by the grains. It is possible that if the form-induced shear stresses were accounted for in the present model, the higher turbulent kinetic energy near the bed could be better simulated. However, one of the objectives of this study was to present a simple means of representing bed roughness in CFD codes (specifically FLUENT) without requiring code modification through the introduction of user-defined functions. The resulting velocity profiles still appear reasonable, even without modelling the form-induced shear stresses.

Future research could focus on determining how to model these form-induced shear stresses, following the approach of Nikora *et al*. (2001). Nikora *et al*. (2001) cited the lack of appropriate data sets and the associated difficulties in obtaining representative data sets that would allow the quantification of these shear stresses. With technologies such as particle image velocimetry (PIV), appropriate data sets could be collected in a laboratory or field setting. Alternatively, the approach of Lane *et al*. (2004) was verified using high resolution flow acoustic Doppler velocimetry (ADV) measurements, and accurately modelled near-bed velocities and shear stresses at a fine resolution. These high-resolution model results could provide the necessary data to establish valid spatially averaged velocity profiles and determine the magnitude of the form-induced shear stresses, although if appropriate velocity data could be collected at a high enough resolution, it would be preferable to utilize these data in lieu of the output from another model. These data could then be used to guide parameterization of the shear stresses. In this paper, the field-measured velocity profiles of Marchand *et al*. (1984) were averaged from three or four locations in the stream and considered representative of the spatial variability of the data. Using more complete data sets would remove some of the uncertainty in the spatially averaged velocity profiles and allow a more accurate understanding of the differences in model results.

The RNG k–ε turbulence model was used for this study. In some cases, it may be desirable to avoid the assumptions of turbulence isotropy associated with two-equation turbulence models and use a higher order turbulence closure to more accurately capture secondary currents in the flow. In other cases, the standard k–ε model may be applied if the RNG k–ε model is unavailable with a specific CFD modelling application. Preliminary comparisons between model results using the standard k–ε, the RNG k–ε, and the second-order seven-equation Reynolds stress model turbulence closures revealed differences in the resulting profiles, mostly in the magnitude of the resulting flows. With the present porous treatment of the bed, the RNG k–ε turbulence closure appeared to most accurately represent the flow profiles. Additional research should be conducted if the porous representation of the bed is coupled with an alternative turbulence model to assess the effects of turbulence closure on model results.

The porous bed representation computes spatially averaged characteristics of the flow and, therefore, the variability in the velocity fields at different locations in the flow will not be captured. However, this model could provide a means of representing rough beds in future CFD modelling of stream reaches, depending on the resolution of velocities that are needed. In applying this methodology on the reach scale, the porous treatment of the bed would represent the roughness due to the bed grains and traditional survey data could be used to capture large-scale topographic features such as pool–riffle sequences and other geomorphic features. The distinction between the large-scale roughness features that should be included in the modelled topography versus what is represented in the porous treatment of the bed is not entirely clear. Similar difficulties have been identified related to a roughness length treatment of the bed (Nicholas and Sambrook-Smith, 1999). There is a need to address this question in future research.

The majority of CFD studies of natural streams assume either a smooth bed or utilize the traditional wall function approach with a roughness length (e.g. Nicholas and Sambrook-Smith, 1999; Booker *et al*., 2001; Ferguson *et al*., 2003). This porous treatment of the bed could facilitate the investigation of complex flow scenarios in gravel-bed streams that have only been examined with relatively smooth boundary assumptions in the past. The present study focused on spatially averaged two-dimensional flow profiles; further research could demonstrate the extension of the methodology to more complex three-dimensional scenarios.

Buffington and Montgomery (1999) mapped the variability of surface textures in stream reaches to aid in understanding the influence of large woody debris (LWD) and vegetation on surface heterogeneity, and availability of aquatic habitat. Differences in surface texture could be included in CFD applications through the use of the porous zone treatment of the bed. In doing so, the effects of distinct roughness patches could be investigated.

Olsen and Stokseth (1995) applied a similar porosity treatment of the boundary in CFD in order to represent large roughness elements in a river. Numerous investigators have developed models to represent vegetation in CFD based on drag forces (Lopez and Garcia, 1997; Fischer-Antze *et al*., 2001). The concept of computing a drag force for a given object in the flow, the basis of the method presented in this study, could be extended to include other roughness elements in CFD studies, such as boulders, LWD, or vegetation in a stream.

Conclusion

The results of this analysis indicate that representing the bed of rough natural channels as a porous zone is a reasonable and straightforward alternative to the standard roughness length treatment. The method proposed by Wiberg and Smith (1991) for representing spatially averaged velocity profiles was modified for use in CFD and applied to model streams with high relative roughness (up to $D_{84}/h = 0{\cdot}3$) and high gradients (up to $S_o = 0{\cdot}029$ m/m), yielding reasonable agreement between model results and field measurements of velocity profiles. This approach also reproduced the non-logarithmic behaviour of the average velocity profiles in these streams. Patterns in the modelled turbulent kinetic energy are consistent with previous modelling and field observations, including simulating a peak in the turbulent kinetic energy around $0{\cdot}2\ h$. High turbulent kinetic energy directly adjacent to the bed, observed by some researchers, is not captured in this modelling scheme. It appears that these high turbulent kinetic energy levels are the result of spatial variability near the bed, and could potentially be incorporated into the model.

This method frees CFD modelling from the constraints imposed by a roughness length treatment of the bed. The method does not reproduce the kind of flow detail of Lane *et al*. (2004) because of the spatial averaging, yet the method is not nearly as data intensive. The method appears to produce velocity profiles of a similar accuracy to the Lane (2005) drag force methodology, yet is based on grain size distributions rather than bed surface profiles, which are easier to measure in the field. In FLUENT, the method can be implemented using built-in capabilities through the use of porous media. The porous bed treatment of roughness could be applied to investigate a wide variety of cases involving beds with large relative roughness that have not been studied in the past due to challenges in CFD modelling.

References

Bathurst JC, Li RM, Simons DB. 1981. Resistance equation for large-scale roughness. *Journal of the Hydraulics Division, ASCE, Proceedings* **27**(HY12): 1593–1613.

Booker DJ. 2003. Hydraulic modelling of fish habitat in urban rivers during high flows. *Hydrological Processes* **17**: 577–599.

Booker DJ, Sear DA, Payne AJ. 2001. Modelling three-dimensional flow structures and patterns of boundary shear stress in a natural pool-riffle sequence. *Earth Surface Processes and Landforms* **26**: 553–576.

Bradbrook KF, Biron P, Lane SN, Richards KS, Roy AG. 1998. Investigation of controls on secondary circulation in a simple confluence geometry using a three-dimensional numerical model. *Hydrological Processes* **12**: 1371–1396.

Bray DI. 1982. Flow resistance in gravel bed rivers. In *Gravel Bed Rivers*, Hey RD, Bathurst JC, Thorne CR (eds). Wiley: Chichester; 109–137.

Buffin-Belanger T, Roy AG. 1998. Effects of a pebble cluster on the turbulent structure of a depth-limited flow in a gravel-bed river. *Geomorphology* **25**: 249–267.

Buffington JM, Montgomery DR. 1999. A procedure for classifying textural facies in gravel-bed rivers. *Water Resources Research* **35**(6): 1903–1914.

Butler JB, Lane SN, Chandler JH. 2001. Characterization of the structure of river-bed gravels using two-dimensional fractal analysis. *Mathematical Geology* **33**: 301–330.

Cebeci T, Bradshaw P. 1977. *Momentum Transfer in Boundary Layers*. Hemisphere Publishing Corporation: New York.

Clifford NJ, Robert A, Richards KS. 1992. Estimation of flow resistance in gravel-bedded rivers: A physical explanation of the multiplier of roughness length. *Earth Surface Processes and Landforms* **17**: 111–126.

Coleman NL. 1967. A theoretical and experimental study of drag and lift forces acting on a sphere resting on a hypothetical streambed. *Proceedings of the 12th Congress*, Vol. 3. International Association of Hydraulic Research: 185–192.

Engelund F. 1953. On the laminar and turbulent flows of groundwater through homogeneous sand. *Transactions of the Danish Academy of Technical Sciences* **3**.

Ferguson RI, Parsons DR, Lane SN, Hardy RJ. 2003. Flow in meander bends with recirculation at the inner bank. *Water Resources Research* **39**(11): Art. No. 1322. DOI: 10.1029/2003WR001965.

Fischer-Antze T, Stoesser T, Bates P, Olsen NRB. 2001. 3D numerical modelling of open-channel flow with submerged vegetation. *Journal of Hydraulic Research* **39**(3): 303–310.

Fluent Inc. 2003. *Fluent 6.1 User's Guide*. Fluent Inc.: Lebanon, NH.

Hardy RJ, Lane SN, Ferguson RI, Parsons D. 2003. Assessing the credibility of a series of computational fluid dynamic simulations of open channel flow. *Hydrological Processes* **17**(8): 1539–1560.

Hey RD. 1979. Flow resistance in gravel-bed rivers. *Journal of the Hydraulics Division, ASCE* **105**: 365–379.

Lane SN, Bradbrook KF, Richards KS, Biron PA, Roy AG. 1999. The application of computational fluid dynamics to natural river channels: Three-dimensional versus two-dimensional approaches. *Geomorphology* **29**: 1–20.

Lane SN, Hardy RJ, Elliott L, Ingham DB. 2004. Numerical modeling of flow processes over gravelly surfaces using structured grids and a numerical porosity treatment. *Water Resources Research* **40**(1): Art. No. W01302. DOI: 10.1029/2002WR001934.

Lawless M, Robert A. 2001. Three-dimensional flow structure around small-scale bedforms in a simulated gravel-bed environment. *Earth Surface Processes and Landforms* **26**: 507–522.

Limerinos JT. 1970. *Determination of the Manning coefficient from measured bed roughness in natural channels*. US Geological Survey Water Supply Paper, 1898-B.

Lopez F, Garcia MH. 1997. *Open-channel flow through simulated vegetation: Turbulence modeling and sediment transport*. Wetlands Research Program Technical Report WRP-CP-10. US Army Corps of Engineers, Waterways Experiment Station: Vickburg, MS.

Marchand JP, Jarrett RD, Jones LL. 1984. *Velocity profile, water-surface slope, and bed-material size for selected streams in Colorado*. US Geological Survey Open File Report, 84-733.

Nicholas AP. 2001. Computational fluid dynamics modelling of boundary roughness in gravel-bed rivers: An investigation of the effects of random variability in bed elevation. *Earth Surface Processes and Landforms* **26**: 345–362.

Nicholas AP. 2005. Roughness parameterization in CFD modelling of gravel-bed rivers. In *Computational Fluid Dynamics: Applications in Environmental Hydraulics*, Bates PD, Lane SN, Ferguson RI (eds.), John Wiley and Sons: Chichester. 540.

Nicholas AP, McLelland SJ. 2004. Computational fluid dynamics modelling of three-dimensional processes on natural river floodplains. *Journal of Hydraulic Research* **42**(2): 131–143.

Nicholas AP, Sambrook-Smith GH. 1999. Numerical simulation of three-dimensional flow hydraulics in a braided channel. *Hydrological Processes* **13**: 913–929.

Nikora V, Goring D, McEwan I, Griffiths G. 2001. Spatially averaged open-channel flow over rough bed. *Journal of Hydraulic Engineering, ASCE* **127**(2): 123–133.

Nikuradse J. 1933. *Laws for flows in rough pipes* NACA Technical Memorandum, 1292 (in German).

Nowell ARM, Church M. 1979. Turbulent flow in a depth-limited boundary layer. *Journal of Geophysical Research* **84**: 4816–4824.

Olsen NRB, Stokseth S. 1995. Three-dimensional numerical modelling of water flow in a river with large bed roughness. *Journal of Hydraulic Research* **33**(4): 571–581.

Raupach MR, Shaw RH. 1982. Averaging procedures for flow within vegetated canopies. *Boundary Layer Meteorology* **22**: 79–90.

Shimizu Y, Tsujimoto T. 1994. Numerical analysis of turbulent open channel flow over a vegetation layer using a k–ε turbulence model. *Journal of Hydroscience and Hydraulic Engineering* **11**(2): 57–67.

Wang JJ, Chen CZ, Dong ZN, Xia ZH. 1993. The effects of bed roughness on the distribution of turbulent intensities in open channel flow. *Journal of Hydraulic Research* **31**(1): 89–98.

Whiting PJ, Dietrich WE. 1990. Boundary shear stress and roughness over mobile alluvial beds. *Journal of Hydraulic Engineering, ASCE* **116**(12): 1495–1511.

Wiberg PL, Smith JD. 1991. Velocity distribution and bed roughness in high gradient streams. *Water Resources Research* **27**(5): 825–838.

Wilcock PR. 1996. Estimating local bed shear stress from velocity distributions. *Water Resources Research* **32**(11): 3361–3366.

Yakhot V, Orszag SA. 1986. Renormalization group analysis of turbulence: I. Basic Theory. *Journal of Scientific Computing* **1**: 1–51.

